A Model for Heat Transfer From Embedded Blood Vessels in Two-Dimensional Tissue Preparations

Liang Zhu

Sheldon Weinbaum

Department of Mechanical Engineering,
The City College of the
City University of New York,
New York, NY 10031

Two-dimensional microvascular tissue preparations have been extensively used to study blood flow in the microcirculation, and, most recently, the mechanism of thermal equilibration between thermally significant countercurrent artery-vein pairs. In this paper, an approximate three-dimensional solution for the heat transfer from a periodic array of blood vessels in a tissue preparation of uniform thickness with surface convection is constructed using a newly derived fundamental solution for a Green's function for this flow geometry. This approximate solution is exact when the ratio K′ of the blood to tissue conductivity is unity and a highly accurate approximation when K′ ≠ 1. This basic solution is applied to develop a model for the heat transfer from a countercurrent artery-vein pair in an exteriorized rat cremaster muscle preparation. The numerical results provide important new insight into the design of microvascular experiments in which the axial variation of the thermal equilibration in microvessels can be measured for the first time. The solutions also provide new insight into the design of fluted fins and microchips that are convectively cooled by internal pores.

1 Introduction

The heat exchange between countercurrent microvascular artery-vein pairs has attracted widespread attention since the combined theoretical and experimental studies by the authors [1, 2, 3] first suggested that this might be the dominant heat transfer mechanism in local microvascular blood-tissue heat transfer. Earlier theoretical predictions by Chen and Holmes [4] and Chato [5] had shown that thermal equilibration between blood and tissue occurred primarily in vessels that were 50 to 500 μm diameter. The experiments in [3], in which the thermal disturbances in the vicinity of these vessels were measured by high resolution fine wire thermocouples in a cross-sectional plane, showed that microvascular artery-vein temperature differences in these primary heat exchange vessels were only of the order of 0.1 to 0.2°C for vessels 100 μm dia or larger, whereas for vessels less than 50 μm dia there were no measurable disturbances. While this experimental evidence strongly supports the hypothesis in [1, 2] as to the importance of countercurrent microvascular heat exchange, there has been no experimental study that has measured the axial thermal equilibration length for different size microvessels in an in vivo or in situ tissue preparation. The two-dimensional tissue preparations described in this study should lead to the first direct measurement of this axial thermal equilibration and a direct confirmation of the countercurrent heat exchange hypothesis for microcirculatory flow.

Contributed by the Bioengineering Division for publication in the JOURNAL OF BIOMECHANICAL ENGINEERING. Manuscript received by the Bioengineering Division March 29, 1993; revised manuscript received October 28, 1993. Associate Technical Editor: R. Roemer.

Microvascular blood flow is commonly examined in a variety of two-dimensional tissue preparations, rabbit ear, frog mesentery, rat cremaster muscle, hamster cheek pouch, to mention a few of the more widely used preparations. Such tissue specimens are nearly transparent, of uniform thickness and the flow in several successive generations of vessels can be examined. In this paper, a theory for blood-tissue heat transfer in these two-dimensional tissue preparations will be presented. A simplified fundamental solution for a single vessel in a periodic array of vessels will first be constructed using a newly derived Green's function for this flow geometry. We shall demonstrate that this solution is exact when the ratio of blood to tissue conductivity $K' = 1$ and show, by comparison with an exact solution for a single vessel in a periodic array, that this solution is highly accurate when $K' \neq 1$ for a wide range of vessel eccentricities and surface Biot numbers Bi. We shall then construct a model for countercurrent axial heat exchange in a thin tissue layer by the superposition of this simplified fundamental solution. The latter model will then be applied to predict the thermal equilibration in first and second generation vessels of an exteriorized rat cremaster muscle preparation. These predictions are currently being used by the authors to design an experiment in which one can obtain the first direct in situ measurements of microvascular countercurrent axial thermal equilibration in perfused tissue using high resolution infra-red thermography.

Countercurrent and periodic array heat transfer from embedded tubes has been extensively studied in applications involving buried pipes, solar collectors and fluted fins. The last model geometry is shown in Fig. 1. This type of enhanced

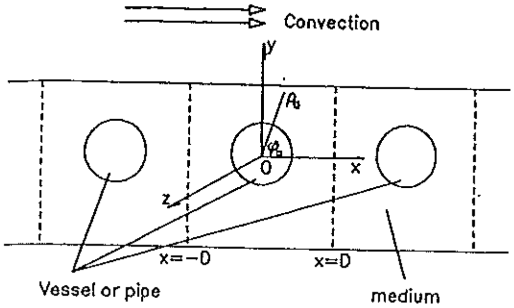

Fig. 1 Schematic of vessels or pipes embedded in surrounding medium with surface convection

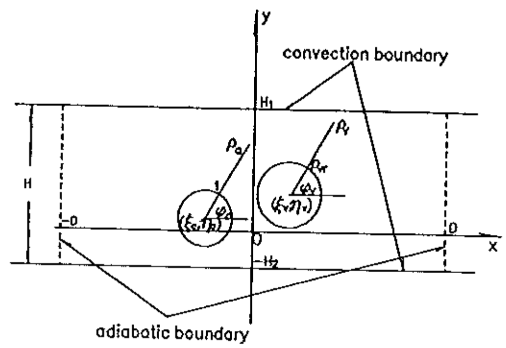

Fig. 2 The geometry of the cross-sectional plane and coordinate system for two vessels

cooling has been considered for microchips subject to high heat loads in the computer industry. The above applications have motivated many previous theoretical studies. The problem of a single tube in a semi-infinite medium with uniform temperature or uniform heat flux boundary conditions is considered in [6, 7]. These solutions were extended to nonuniform free surface convective boundary conditions for a buried pipe in a semi-infinite medium using conformal mapping techniques by Bau and Sadhal [8]. This approach was also used by DiFelice and Bau [9] to describe the convective heat transfer between two buried pipes in an infinite medium.

Recent interest in modeling countercurrent vessels in perfused tissue and limbs has motivated several recent solutions for two vessels (equal or unequal) embedded in a cylinder in which both the vessels and the cylinder surface were at constant temperature in the cross-sectional plane [10, 11]. Zhu et al. [12] treated a similar problem but developed a new solution approach for vessels with small eccentricity, which allowed both the vessels and the cylinder surface to have axially varying nonuniform convective boundary conditions. The latter theory was an extension of the exact solution of Wissler [13] for the perfect countercurrent heat transfer between two vessels with parabolic flow profiles and nonuniform wall temperature in an infinite medium, where the artery, vein and tissue had the same linear axial temperature gradient. Recently, Wu et al. [14] have constructed a new analytic solution approach for treating any finite number of vessels arbitrarily placed in a cylinder with surface convection. This last solution can be used to more realistically model the heat transfer between the major axial arteries and veins in the limb, since it is not limited to small eccentricities. This solution, like the solution generated in the present paper, is exact when $K' = 1$ and highly accurate when $K' \neq 1$.

The boundary conditions for embedded vessels in a thin tissue slab do not allow for an analytic solution approach of the type presented in [14]. In the latter study one could use a superposition of solutions that collectively, but not individually, satisfied the convective conditions at the cylinder surface. In contrast, the mixed rectangular and cylindrical coordinates and the mixed boundary conditions describing the periodic rectangular geometry in Fig. 1 do not allow this type of approach. Instead, we shall derive a fundamental solution or Green's function that already satisfies all the conditions on the outer boundary, and then construct a superposition that satisfies the matching conditions on the vessel surface. In Section 2 we formulate the general problem. In Sections 3A and 3B we present approximate and exact solutions for the periodic geometry in Fig. 1 and in Section 4 we will generalize these results for two or more vessels. Results and discussion are presented in Section 5.

2 Formulation

For the general case we consider two or more vessels embedded in a thin tissue layer of thickness $H = H_1 + H_2$, as shown in Fig. 2. A steady-state temperature field is assumed in both the vessels and the surrounding tissue. The axes of the vessels are perpendicular to the plane of the figure in the z direction. It is assumed that the velocity

Nomenclature

a, b = coefficients for vessel solution in Eqs. (10), (31), and (32)
Bi = Biot number, $h\rho_{ar}^*/K_t$
C = constant in Eq. (26)
Cp = specific heat of blood
C_{sa}, C_{sv} = source strength
D = half width of tissue
h = thermal convection coefficient
H = total thickness of tissue
K = thermal conductivity
K' = ratio of conductivities of vessel to tissue
Nu = Nusselt number defined in Eq. (23)
q_a = heat transfer per unit length of vessel in Eq. (21)
Pe = Peclet number of vessel
r = radial coordinate
Sa = eccentricity of vessel in tissue
T = temperature
V = average blood flow velocity
$\bar{V}$ = ratio of V_v to V_a
W = Green's function
x, y, z = Cartesian coordinates in Fig. 2
Γ = boundary in Eq. (26)
γ = density
θ = dimensionless temperature
λ = eigenvalue in Eqs. (14) and (33)
ξ, η = Cartesian coordinate
ρ = radial coordinate
ρ_{vr} = dimensionless radius of vein
σ = shape factor
ϕ, ψ = polar angle in cylindrical coordinate
Ω = domain inside boundary Γ

Subscripts

a = artery (or single vessel)
b = bulk
f = fluid in vessels
h = homogeneous temperature
p = particular solution
s = source
t = tissue
v = vein
w = wall
1,2 = upper and lower surfaces

profile in the vessels is parabolic and the Peclet number $>> 1$. Thus, if the vessel length $L >> H$, axial conduction and end effects can be neglected [12].

The nondimensional parameters are introduced as follows:

$$\rho_a = \frac{\rho_a^*}{\rho_{ar}^*},\ \rho_v = \frac{\rho_v^*}{\rho_{ar}^*},\ \rho_{vr} = \frac{\rho_{vr}^*}{\rho_{ar}^*},\ x = \frac{x^*}{\rho_{ar}^*},\ y = \frac{y^*}{\rho_{ar}^*},$$

$$z = \frac{z^*}{\rho_{ar}^* \mathrm{Pe}},\ H_{1,2} = \frac{H_{1,2}^*}{\rho_{ar}^*},\ D = \frac{D^*}{\rho_{ar}^*},\ \mathrm{Pe} = \frac{2\gamma_f C p_f \rho_a^* V_a}{K_f},$$

$$\mathrm{Bi}_{1,2} = \frac{h_{1,2}\,\rho_{ar}^*}{K_t},\ \theta_{a,v,t} = \frac{T_{a,v,t} - T_\infty}{T_{a0} - T_\infty},\ \bar{V} = \frac{V_v}{V_a}$$

here the subscripts a, v refer to artery and vein, asterisks denote dimensional variables, and ρ_{ar}^* and ρ_{vr}^* are the dimensional radii of the artery and vein. This coordinate system is sketched in Fig. 2. To simplify the analysis, we assume that the temperature gradient $\partial\theta_{a,v}/\partial z$ in the convective term of the vessel energy equations can be approximated by the axial gradient of the vessel bulk temperatures, $d\theta_{ab,vb}/dz$ as previously justified in [12]. The simplified dimensionless governing equations and boundary conditions for the vessels and the tissue are

$$\frac{1}{\rho_a}\frac{\partial}{\partial\rho_a}\left(\rho_a\frac{\partial\theta_a}{\partial\rho_a}\right) + \frac{1}{\rho_a^2}\frac{\partial^2\theta_a}{\partial\phi_a^2} = \left(1-\rho_a^2\right)\frac{d\theta_{ab}}{dz},\quad \rho_a \le 1 \tag{1}$$

$$\frac{1}{\rho_v}\frac{\partial}{\partial\rho_v}\left(\rho_v\frac{\partial\theta_v}{\partial\rho_v}\right) + \frac{1}{\rho_v^2}\frac{\partial^2\theta_v}{\partial\phi_v^2} = \bar{V}\left(1-\frac{\rho_v^2}{\rho_{vr}^2}\right)\frac{d\theta_{vb}}{dz},\quad \rho_v \le \rho_{vr} \tag{2}$$

$$\frac{\partial^2\theta_t}{\partial x^2} + \frac{\partial^2\theta_t}{\partial y^2} = 0,$$

$$\rho_a > 1,\ \rho_v > \rho_{vr},\ -D \le x \le D,\ -H_2 \le y \le H_1 \tag{3}$$

$$\theta_a = \theta_t,\quad \rho_a = 1 \tag{4a}$$

$$K'\frac{\partial\theta_a}{\partial\rho_a} = \frac{\partial\theta_t}{\partial\rho_a},\quad \rho_a = 1 \tag{4b}$$

$$\theta_v = \theta_t,\quad \rho_v = \rho_{vr} \tag{5a}$$

$$K'\frac{\partial\theta_v}{\partial\rho_v} = \frac{\partial\theta_t}{\partial\rho_v},\quad \rho_v = \rho_{vr} \tag{5b}$$

$$\frac{\partial\theta_t}{\partial y} = -\mathrm{Bi}_1\theta_t,\quad y = H_1 \tag{6a}$$

$$\frac{\partial\theta_t}{\partial y} = \mathrm{Bi}_2\theta_t,\quad y = -H_2 \tag{6b}$$

For a periodic array of equally spaced vessels, as shown in Fig. 1, there is no heat flow across the boundaries at $x = \pm D$. For vessel pairs whose spacing between pairs $2D$ is much larger than the tissue thickness H, this no flux boundary condition is also closely approximated. Thus, for either case we shall require the adiabatic condition:

$$\frac{\partial\theta_t}{\partial x} = 0\quad x = \pm D \tag{7}$$

In Eqs. (1) and (2), θ_{ab} and θ_{vb} are the artery and vein bulk temperatures that are defined as

$$\theta_{ab} = \frac{2}{\pi}\int_{-\pi}^{\pi}\int_0^1 \theta_a\left(1-\rho_a^2\right)\rho_a d\rho_a d\phi_a \tag{8}$$

$$\theta_{vb} = \frac{2}{\pi\rho_{vr}^2}\int_{-\pi}^{\pi}\int_0^{\rho_{vr}} \theta_v\left(1-\frac{\rho_v^2}{\rho_{vr}^2}\right)\rho_v d\rho_v d\phi_v \tag{9}$$

3 Solution for Single Vessel

In this section, two solutions are constructed for the temperature field within and surrounding a single vessel in a periodic array of blood vessels for the flow and tissue geometry depicted in Fig. 1. The first employs a newly derived Green's function or fundamental solution that is placed at the origin of each vessel. This solution is exact only when $K' = 1$. The second is a significantly more complicated solution using an integral equation formulation of this Green's function. This latter solution is exact for all values of K'. The accuracy of the first solution for $K' \neq 1$ is examined by comparing it with the exact integral equation solution. It is shown that the approximate solution for $K' \neq 1$ is also highly accurate for most conditions of interest. The approximate solution is, therefore, used to construct the more general solution in Section 4 for two or more eccentrically located vessels, shown in Fig. 2.

A Approximate Solution. The governing equations and boundary conditions for a single vessel are Eqs. (1), (3), (4), (6), (7). The solution of Eq. (1) for the vessel temperature θ_a can be decomposed into two parts, a particular solution θ_{pa} and a general solution θ_{ha} in the form of a Fourier series, whose superposition is given by

$$\theta_a = \left(\rho_a^2 - \frac{1}{4}\rho_a^4 - \frac{3}{4}\right)\frac{1}{4}\frac{d\theta_{ab}}{dz} + \frac{a_{a0}}{2} + \sum_{j=1}^{\infty} a_{aj}\rho_a^j\cos(j\phi_a) \tag{10}$$

Since j is a positive integer, this solution has no singular point.

We assume that the tissue temperature field can be constructed by placing an anisotropic line source of strength C_{sa} at the center of each vessel in the periodic array. This fundamental solution is given by

$$\theta_t = C_{sa}W(x,y;0,0) \tag{11}$$

where W is a Green's function, which satisfies Laplace's equation in the rectangular region, $-D \le x \le D$ and $-H_2 \le y \le H_1$, except for the source point (0,0) at the center of the vessel, and the boundary conditions (6) and (7). The boundary value problem for this singular solution is

$$\frac{\partial^2 W}{\partial x^2} + \frac{\partial^2 W}{\partial y^2} = \delta(x-\xi)\delta(y-\eta) \tag{12}$$

$$\frac{\partial W}{\partial x} = 0\qquad \text{at } x = \pm D \tag{13a}$$

$$\frac{\partial W}{\partial y} = -\mathrm{Bi}_1 W\qquad \text{at } y = H_1 \tag{13b}$$

$$\frac{\partial W}{\partial y} = \mathrm{Bi}_2 W\qquad \text{at } y = -H_2 \tag{13c}$$

where (ξ,η) are the coordinates of the source point. The solution to (12) and (13) for the Green's function $W(x,y;0,0)$ is given in Appendix 1 by Eq. (A.12).

$$W = (C_1 y + C_2) + \sum_{n=1}^{\infty}\frac{1}{D}\cos\left[\frac{n\pi}{2}\right]$$
$$\times\cos\left[\sqrt{\lambda_n}(x-D)\right]\left[A_1 e^{\sqrt{\lambda_n}y} + B_1 e^{-\sqrt{\lambda_n}y}\right]\quad y \ge 0 \tag{14a}$$

$$W = (D_1 y + D_2) + \sum_{n=1}^{\infty} \frac{1}{D} \cos\left[\frac{n\pi}{2}\right]$$

$$\times \cos\left[\sqrt{\lambda_n}(x-D)\right]\left[A_2 e^{\sqrt{\lambda_n} y} + B_2 e^{-\sqrt{\lambda_n} y}\right] \quad y \le 0 \quad (14b)$$

where the A_i, B_i, C_i, D_i, $i = 1,2$ are constants, which depend on the Biot number and the tissue geometry, and are listed in ($A.8$) and ($A.10$) of Appendix 1 and the eigenvalues $\lambda_n = (n\pi/2D)^2$.

The coefficients a_{aj} in Eq. (10) for the vessel temperature are determined by the matching conditions (4) for the continuity of temperature and heat flux on the vessel surface. For temperature continuity,

$$C_{sa} W(x,y{:}0,0)|_{\rho_a=1} = \left(\rho_a^2 - \frac{1}{4}\rho_a^4 - \frac{3}{4}\right)\frac{1}{4}\frac{d\theta_{ab}}{dz} + \frac{a_{a0}}{2} + \sum_{j=1}^{\infty}\left[\rho_a^j a_{aj}\cos(j\phi_a)\right]|_{\rho_a=1} \quad (15)$$

where in $W(x,y{:}0,0)$, $x = \rho_a \cos\phi_a$, $y = \rho_a \sin\phi_a$. Multiplying both sides of (15) by $\cos(j\phi_a)$ and integrating from $-\pi$ to π, we obtain

$$a_{a0} = \int_{-\pi}^{\pi}\left[\frac{C_{sa}}{\pi} W(x,y{:}0,0)\right]|_{\rho_a=1} d\phi_a \quad (16a)$$

$$a_{aj} = \int_{-\pi}^{\pi}\left[\frac{C_{sa}}{\pi} W(x,y{:}0,0)\right]\frac{\cos(j\phi_a)}{\rho_a^j}|_{\rho_a=1} d\phi_a$$

$$j = 1,2,\ldots\infty \quad (16b)$$

where the strength of the source C_{sa} still needs to be determined. Continuity of heat flux requires that

$$\left[C_{sa}\frac{\partial W(x,y{:}0,0)}{\partial \rho_a}\right]|_{\rho_a=1} = \frac{K'}{4}\frac{d\theta_{ab}}{dz} + \sum_{j=1}^{\infty}\left[K' j \rho_a^{j-1} a_{aj}\cos(j\phi_a)\right]|_{\rho_a=1} \quad (17)$$

Multiplying both sides of Eq. (17) by $\cos(j\phi_a)$ and integrating from $-\pi$ to π, we obtain

$$C_{sa} = \frac{K'\pi}{2}\frac{d\theta_{ab}}{dz} \quad (18a)$$

$$a_{aj} = \frac{1}{K'}\int_{-\pi}^{\pi}\left[\frac{C_{sa}}{\pi}\frac{\partial W(x,y{:}0,0)}{\partial \rho_a}\right]\frac{\cos(j\phi_a)}{j\rho_a^{j-1}}|_{\rho_a=1} d\phi_a$$

$$j = 1,2,\ldots\infty \quad (18b)$$

Equation (18a) is an integral average constraint requiring that there be a global conservation of energy for the total heat flux crossing the vessel surface $\rho_a = 1$. In contrast, (18b) is a local heat flux condition. Equations (16b) and (18b) provide two independent relations for the a_{aj} coefficients. Thus, for both temperature and heat flux to be continuous locally at $\rho_a = 1$ these two expressions for the a_{aj} must be equal. Equating (16b) and (18b), we have

$$\frac{C_{sa}}{\pi}\int_{-\pi}^{\pi}\left[W(x,y{:}0,0)\frac{K'}{\rho_a^j} - \frac{\partial W(x,y{:}0,0)}{\partial \rho_a}\frac{1}{j\rho_a^{j-1}}\right]$$

$$\times \cos(j\phi_a)|_{\rho_a=1} d\phi_a = 0 \quad j = 1,2,\ldots\infty \quad (19)$$

In Appendix 2, it is shown that (19) is exactly satisfied only when $K' = 1$. The solution given by Eqs. (10), (11), (16), and (18a) is, therefore, exact when $K' = 1$ and approximate when $K' \neq 1$. For $K' \neq 1$ it satisfies the outer boundary conditions since θ_t is proportional to the Green's function (14) which satisfies the outer boundary conditions, while at $\rho_a = 1$ only the continuity of temperature is satisfied locally. However, as will be shown in Section 5 the global constraint on heat flux (18a) provides a very strong compatibility condition and the approximate solution for $K' \neq 1$ is remarkably accurate for nearly all flow conditions of interest.

To complete the analysis we shall obtain expressions for the bulk temperature, the conduction shape factor σ_a and the Nusselt number Nu_a. Substituting (10) into (8), we obtain

$$\theta_{ab} = -\frac{11}{96}\frac{d\theta_{ab}}{dz} + \frac{a_{a0}}{2} \quad (20)$$

where a_{a0} is proportional to $d\theta_{ab}/dz$ from (16a) and (18a). Equation (20) can be integrated axially subject to an entrance condition at $z = 0$. Once $\theta_{ab}(z)$ is known, Eqs. (10) and (11) provide the complete solution for the temperature field in both the vessel and the tissue. The integrals for the a_{aj} in (16) involve only a single integration that requires insignificant computational time.

The shape factor σ_a for heat transfer between a vessel in the periodic array and the tissue layer is defined by

$$\sigma_a = \frac{q_a}{2\pi K_t(T_{ab} - T_\infty)} = -\frac{K'}{4}\frac{\frac{d\theta_{ab}}{dz}}{\theta_{ab}} \quad (21)$$

Here q_a is the heat transfer per unit vessel length and is equal to $-\gamma_f C p_f \pi \rho_{ar}^{*2} V_a (dT_{ab}/dz^*)$. One observes from (20) and (21) that σ_a depends only on the single unknown coefficient a_{a0} which is given by (16a). Thus, substituting (20) into (21) and using (16a) and (18a), one obtains

$$\sigma_a = -\frac{K'}{4}\frac{1}{-\frac{11}{96} + \frac{K'}{2}\int_{-\pi}^{\pi} W(x,y{:}0,0)|_{\rho_a=1} d\phi_a} \quad (22)$$

(22) provides a simple closed from expression for the shape factor σ_a.

The vessel Nusselt number is defined by

$$\mathrm{Nu}_a = \frac{q_a}{\pi K_f(T_{ab} - T_{aw})} = -\frac{1}{2}\frac{\frac{d\theta_{ab}}{dz}}{\theta_{ab} - \theta_{aw}} \quad (23)$$

where, θ_{aw}, the dimensionless mean wall temperature of the vessel, is given by

$$\theta_{aw} = \frac{1}{2\pi}\int_{-\pi}^{\pi}\theta_a(1,\phi_a)d\phi_a = \frac{a_{a0}}{2} \quad (24)$$

Substituting (24) into (23), we obtain

$$\mathrm{Nu}_a = \frac{48}{11} \quad (25)$$

This Nusselt number is the same value as for a fully developed temperature profile in a pipe with constant heat flux to the environment. One can show that the homogeneous terms in the summation in (10) do not contribute to Nu_a.

B Exact Solution for $K' \neq 1$ Using Green's Theorem. Since the solution in Section 3A is exact only when $K' = 1$, we shall also construct for comparison an exact solution, valid for all values of K'. This solution will be based on a generalization of the Green's function (12), which is valid at any point in the domain, and the application of Green's theorem. The resulting integral equation will be reduced to a linear system of matrix equations for the unknown coefficients a_{aj} that appear in (10) after applying the boundary and matching conditions at the vessel surface.

If θ_t satisfies Laplace's equation and $W(x,y{:}\xi,\eta)$ is a Green's function with a source point (ξ,η) located within the tissue region, $-D \le x \le D$ and $-H_2 \le y \le H_1$, then Green's theorem reduces to

$$-\theta_t(x,y) = \frac{1}{C}\oint_\Gamma \left[W(x,y:\xi,\eta)\frac{\partial\theta_t(\xi,\eta)}{\partial n} - \theta_t(\xi,\eta)\frac{\partial W(x,y:\xi,\eta)}{\partial n}\right] d\Gamma \quad (26)$$

where C is a constant, which is equal to 1 if (x,y) is an inner point of the tissue region. When (x,y) is a boundary point, C is given by the formula

$$C = \frac{\text{included interior angle}}{2\pi}$$

The generalization of the Green's function $W(x,y:\xi,\eta)$ which satisfies boundary conditions (13) for a source at any point (ξ,η) is given by Eq. ($A.11$) in Appendix 1. Since the Green's function already satisfies the outer boundary conditions (13), one can show that the integral along the outer boundary, where conditions (13) apply, vanishes and (26) reduces to

$$\theta_t(x,y) = \frac{1}{C}\int_{\Gamma_{\text{vessel}}} \left[\theta_t(\xi,\eta)\frac{\partial W(x,y:\xi,\eta)}{\partial n} - W(x,y:\xi,\eta)\frac{\partial\theta_t(\xi,\eta)}{\partial n}\right] d\Gamma$$

$$= -\frac{1}{C}\int_{-\pi}^{\pi} \left[\theta_t(r_a,\psi_a)\frac{\partial W(x,y:r_a,\psi_a)}{\partial r_a} - W(x,y:r_a,\psi_a)\frac{\partial\theta_t(r_a,\psi_a)}{\partial r_a}\right] r_a|_{r_a=1} d\psi_a \quad (27)$$

where the source point $(\xi,\eta) = (r_a\cos\psi_a,\ r_a\sin\psi_a)$. Since the integral in (27) is along the vessel surface, Eq. 10 for θ_a can be used to evaluate both θ_t and $\partial\theta_t/\partial r_a$ in the integral on the right-hand side of (27). Applying matching conditions ($4a$) and ($4b$), one obtains

$$\theta_t(x,y) = -\frac{1}{C}\int_{-\pi}^{\pi} \left\{ \frac{a_{a0}}{2} + \sum_{n=1}^{\infty} \left[r_a^n a_{an}\cos(n\psi_a)\right]\right\} \times \frac{\partial W(x,y:r_a,\psi_a)}{\partial r_a} - K'W(x,y:r_a,\psi_a) \times \left\{ \frac{1}{4}\frac{d\theta_{ab}}{dz} + \sum_{n=1}^{\infty}\left[n r_a^{n-1} a_{an}\cos(n\psi_a)\right]\right\}|_{r_a=1} d\psi_a \quad (28)$$

Equation (28) is an integral equation to determine the tissue temperature field except that the coefficients a_{an} are unknown. Choosing (x,y) as a point on the vessel surface, i.e., $(x,y) = (\rho_a\cos\phi_a,\ \rho_a\sin\phi_a)|_{\rho_a=1}$ and requiring that the left side of (28) be given by (10), one obtains

$$\frac{a_{a0}}{2} + \sum_{j=1}^{\infty} a_{aj}\cos(j\phi_a) = -2\int_{-\pi}^{\pi} \left\{ \frac{a_{a0}}{2}\frac{\partial W}{\partial r_a} + \sum_{n=1}^{\infty}\cos(n\psi_a) \times a_{an}\left[\frac{\partial W}{\partial r_a} - K'nW\right] - \frac{1}{4}\frac{d\theta_{ab}}{dz}K'W\right\}|_{r_a=1,\rho_a=1} d\psi_a \quad (29)$$

We now multiply both sides of (29) by $\cos(j\phi_a)$ and integrate from $-\pi$ to π. This yields

$$a_{aj} = -\frac{2}{\pi}\int_{-\pi}^{\pi} d\phi_a\cos(j\phi_a)\int_{-\pi}^{\pi}\left\{ \frac{a_{a0}}{2}\frac{\partial W}{\partial r_a} + \sum_{n=1}^{\infty}\cos(n\psi_a) \times a_{an}\left[\frac{\partial W}{\partial r_a} - K'nW\right] - \frac{1}{4}\frac{d\theta_{ab}}{dz}K'W\right\}|_{r_a=1,\rho_a=1} d\psi_a$$

$$j = 0,1,2,\ldots\infty \quad (30)$$

Equation (30) is a linear system of algebraic equations for the unknown coefficients a_{aj}. When this system is truncated at $j = M$, we obtain $M+1$ linear equations for the $M+1$ coefficients $a_{a0}\ldots a_{aM}$. When the values of these coefficients are substituted back into (28), we have a full description of the tissue temperature field at any location (x,y). The accuracy of the solution depends on the order of the truncation, but in principle the solution becomes exact as $M \to \infty$.

Although this approach can be used to treat two or more vessels and provides exact results for any value of K', the numerical evaluation of the integral in (30) is very time-consuming, and not convenient for engineering purposes. Therefore, in this paper we shall use (30) only to evaluate the accuracy of the approximate solution in Section 3A when $K' \neq 1$ and use the latter solution to construct the solution for countercurrent vessel pairs.

4 Countercurrent Artery-Vein Pairs

As noted in the introduction, the theory and experiments in [1–5] suggest that in the microcirculation countercurrent artery-vein pairs are the primary blood-tissue heat transfer unit. We would, therefore, like to extend the solution approach in Section 3A to two vessels undergoing countercurrent heat exchange. In nearly all two-dimensional tissue preparations the average spacing of vessel pairs 2D is much larger than the tissue thickness H and, thus, the interaction between vessel pairs can be neglected. The cross sectional geometry and the coordinate system are shown in Fig. 2.

Following the procedure for the single vessel, we write the solution for a countercurrent artery-vein pair as

$$\theta_a = \left(\rho_a^2 - \frac{1}{4}\rho_a^4 - \frac{3}{4}\right)\frac{1}{4}\frac{d\theta_{ab}}{dz} + \frac{a_{a0}}{2} + \sum_{j=1}^{\infty} a_{aj}\rho_a^j\cos(j\phi_a) + b_{aj}\rho_a^j\sin(j\phi_a) \quad (31)$$

$$\theta_v = \left(\rho_v^2 - \frac{1}{4}\frac{\rho_v^4}{\rho_{vr}^2} - \frac{3}{4}\rho_{vr}^2\right)\frac{\bar{V}}{4}\frac{d\theta_{vb}}{dz} + \frac{a_{v0}}{2} + \sum_{j=1}^{\infty} a_{vj}\rho_v^j\cos(j\phi_v) + b_{vj}\rho_v^j\sin(j\phi_v) \quad (32)$$

where, due to the eccentricity of the vessel location, terms involving $\sin(j\phi)$ in both (31) and (32) cannot be omitted as in Eq. (10) for a single vessel.

Using the same technique as in Section 3A, we position two sources of strength C_{sa} and C_{sv} at the centers of the artery and vein, respectively. The tissue temperature is then a linear combination of Green's functions representing these sources and is expressed by

$$\theta_t = C_{sa}W(x,y:\xi_a,\eta_a) + C_{sv}W(x,y:\xi_v,\eta_v) \quad (33)$$

where $W(x,y:\xi,\eta)$ is the more general fundamental solution ($A.11$) in Appendix 1 and is given by

$$W = (C_1y + C_2) + \sum_{n=1}^{\infty}\frac{1}{D}\cos\left[\sqrt{\lambda_n}(\xi - D)\right] \times\cos\left[\sqrt{\lambda_n}(x - D)\right]\left[A_1e^{\sqrt{\lambda_n}y} + B_1e^{-\sqrt{\lambda_n}y}\right] \quad y \ge \eta \quad (33a)$$

$$W = (D_1 y + D_2) + \sum_{n=1}^{\infty} \frac{1}{D} \cos\left[\sqrt{\lambda_n}(\xi - D)\right]$$

$$\times \cos\left[\sqrt{\lambda_n}(x - D)\right]\left[A_2 e^{\sqrt{\lambda_n} y} + B_2 e^{-\sqrt{\lambda_n} y}\right] \quad y < \eta \quad (33b)$$

The coefficients a_{aj}, b_{aj}, a_{vj}, b_{vj}, C_{sa}, and C_{sv} are evaluated in the same manner as for the single vessel in (16) and (18). We only list the final expressions.

$$C_{sa} = \frac{K'\pi}{2} \frac{d\theta_{ab}}{dz} \quad (34a)$$

$$C_{sv} = \frac{K'\pi\rho_{vr}^2 \bar{V}}{2} \frac{d\theta_{vb}}{dz} \quad (34b)$$

$$a_{a0} = \int_{-\pi}^{\pi} \left[\frac{C_{sa}}{\pi} W(x,y:\xi_a,\eta_a) + \frac{C_{sv}}{\pi} W(x,y:\xi_v,\eta_v)\right]\Big|_{\rho_a=1} d\phi_a \quad (34c)$$

$$a_{aj} = \int_{-\pi}^{\pi} \left[\frac{C_{sa}}{\pi} W(x,y:\xi_a,\eta_a) + \frac{C_{sv}}{\pi} W(x,y:\xi_v,\eta_v)\right] \times \frac{\cos(j\phi_a)}{\rho_a^j}\Big|_{\rho_a=1} d\phi_a \quad j = 1,2,\ldots\infty \quad (34d)$$

$$b_{aj} = \int_{-\pi}^{\pi} \left[\frac{C_{sa}}{\pi} W(x,y:\xi_a,\eta_a) + \frac{C_{sv}}{\pi} W(x,y:\xi_v,\eta_v)\right] \times \frac{\sin(j\phi_a)}{\rho_a^j}\Big|_{\rho_a=1} d\phi_a \quad j = 1,2,\ldots\infty \quad (34e)$$

$$a_{v0} = \int_{-\pi}^{\pi} \left[\frac{C_{sa}}{\pi} W(x,y:\xi_a,\eta_a) + \frac{C_{sv}}{\pi} W(x,y:\xi_v,\eta_v)\right]\Big|_{\rho_v=\rho_{vr}} d\phi_v \quad (34f)$$

$$a_{vj} = \int_{-\pi}^{\pi} \left[\frac{C_{sa}}{\pi} W(x,y:\xi_a,\eta_a) + \frac{C_{sv}}{\pi} W(x,y:\xi_v,\eta_v)\right] \times \frac{\cos(j\phi_v)}{\rho_v^j}\Big|_{\rho_v=\rho_{vr}} d\phi_v \quad j = 1,2,\ldots\infty \quad (34g)$$

$$b_{vj} = \int_{-\pi}^{\pi} \left[\frac{C_{sa}}{\pi} W(x,y:\xi_a,\eta_a) + \frac{C_{sv}}{\pi} W(x,y:\xi_v,\eta_v)\right] \times \frac{\sin(j\phi_v)}{\rho_v^j}\Big|_{\rho_v=\rho_{vr}} d\phi_v \quad j = 1,2,\ldots\infty \quad (34h)$$

As in the single vessel case, the foregoing solution is exact when K' is unity and an accurate approximation when $K' \neq 1$.

To complete the analysis, the bulk temperatures θ_{ab} and θ_{vb} satisfy the coupled equations

$$\theta_{ab} = -\frac{11}{96} \frac{d\theta_{ab}}{dz} + \frac{a_{a0}}{2} \quad (35a)$$

$$\theta_{vb} = -\frac{11}{96} \bar{V} \rho_{vr}^2 \frac{d\theta_{vb}}{dz} + \frac{a_{v0}}{2}. \quad (35b)$$

where a_{a0} and a_{v0} from 34(a,b,c,f) are linear combinations of $d\theta_{ab}/dz$ and $d\theta_{vb}/dz$. The solution of (35a) and (35b) requires the specification of two boundary conditions in the axial direction. For countercurrent flow, these boundary conditions are the prescribed bulk temperatures at the inlets of the vessels. Once the bulk temperatures are determined, (31), (32), and (33) provide the solution for the temperature field in the vessels and the tissue.

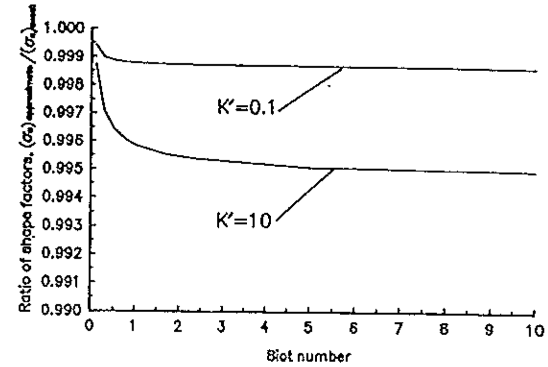

Fig. 3 The effect of Biot number on the accuracy of the shape factor single vessel using the approximate solution in 3A, where $(\sigma_a)_{exact}$ is the result from exact solution in Section 3B, for the case $2D = 20$ and $H = 8$

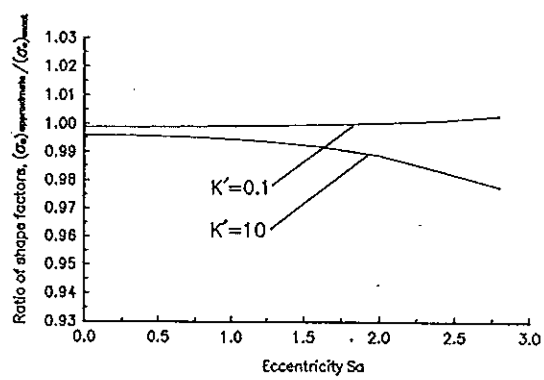

Fig. 4 The effect of vessel eccentricity Sa on the accuracy of the shape factor for a single vessel using the approximate solution for the case $2D = 20$, $Bi_1 = Bi_2 = 1$ and $H = 8$

5 Results and Discussion

(a) Comparison of Approximate and Exact Solutions When $K' \neq 1$. In Figs. 3 and 4 we compare the predictions of the approximate and exact solutions for the shape factor σ_a when $K' \neq 1$ for two extreme cases, $K' = 10$ and $K' = 0.1$, for a single periodically spaced vessel, as shown in Fig. 1. The tissue thickness H is four times the vessel diameter and the spacing, $2D = 20$, is sufficiently large for vessel-vessel interaction to be small. Figure 3 shows that the accuracy of the approximate solution is better than 0.5 percent for $0.1 < \mathrm{Bi} < 10$ and $0.1 < K' < 10$. Figure 4 shows that the error associated with the eccentricity, $Sa = (H_2 - H_1)/2$, is somewhat larger than that associated with the Biot number Bi. As the eccentricity is increased, the error in the approximate solution increases monotonically reaching a maximum of 3 percent for $K' = 10$, and 0.5 percent for $K' = 0.1$, at $Sa = 2.8$. For this value of Sa the top of the vessel is within 0.2 diameters of the upper surface of the tissue.

(b) Single Vessel Shape Factor. The shape factor for the single periodically spaced vessel is examined for a wide range of the governing parameters, vessel periodicity $2D$, eccentricity Sa and Biot number Bi in Figs. 5, 6, and 7. The effect of vessel periodicity $2D$ is shown in Fig. 5 for four different tissue thicknesses, $H = 2.2$, 4, 8, and for $\mathrm{Bi} = 0.1$, 1 and 10 when $H_1 = H_2$ and $K' = 1$. One observes that the shape factor approaches a constant when $2D/H > 2$ for a wide range of Biot numbers. This indicates that when $D > H$ the interaction between vessels is small and the use of the adiabatic boundary condition (7) for the two-vessel geometry in Fig. 2 will be reasonable, although this boundary condition is not strictly satisfied. For most two-dimensional tissue

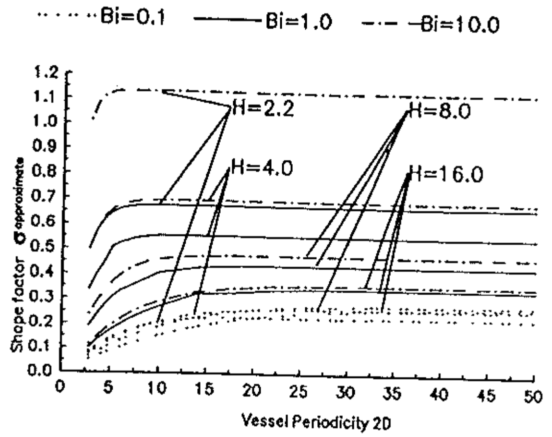

Fig. 5 Shape factor of periodic array of single vessels as a function of vessel periodicity $2D$ for various tissue thicknesses H and Biot numbers Bi. $H_1 = H_2$

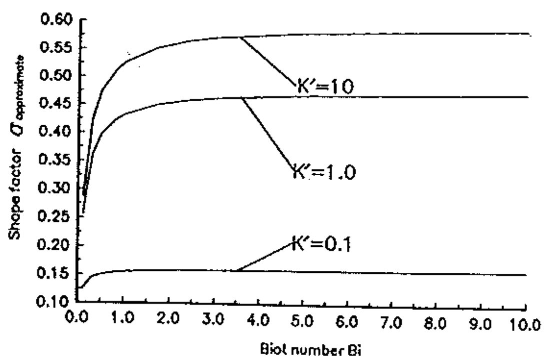

Fig. 6 Shape factor for symmetrically located single vessel as a function of Bi for different K' for $2D = 20$, $H = 8$

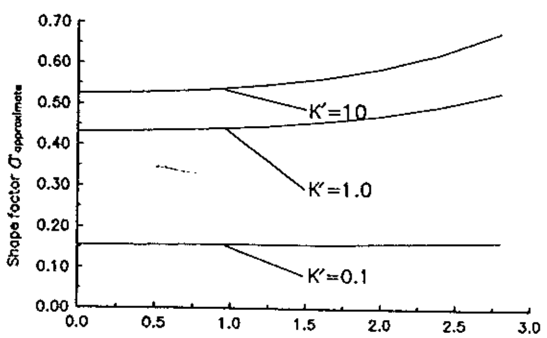

Fig. 7 Shape factor of single vessel as a function for vessel eccentricity Sa for different K' for $2D = 20$, $H = 8$ and $Bi_1 = Bi_2 = 1$

preparations, $2D \gg H$, and H lies between 4 and 8 in the first and second vessel generations. Figure 6 shows how the shape factor varies as a function of Bi for various K' with $H = 8$ and $2D = 20$. Note that the shape factor σ_a is nearly independent of Bi for Bi > 2. The dependence of the shape factor on the eccentricity Sa is shown in Fig. 7 for $H = 8$, $2D = 20$ and Bi = 1. Note that σ_a is a weak function of Sa, but its sensitivity to Sa increases for $K' \gg 1$.

Figures 5, 6, and 7 provide valuable insight into the enhancement in heat transfer that can be achieved by fluted fins and microchips with internal convective pores. One observes from Fig. 5 that for Bi $\ll$ 1, the spacing of the pores or conduits can lead to a roughly fourfold increase in σ_a when $K' = 1$ if $2D$ is increased from the near touching configuration to values where the pores are not interacting with one another. The interaction between pores significantly reduces the heat transfer efficiency of the fin and this behavior is nearly independent of fin thickness H. In contrast, when Bi $\gg$ 1, pore spacing plays a much less significant role. The primary factor is fin thickness, since there is a large conductive resistance in the fin itself. Thus, decreasing H from 8 to 2.2 when Bi = 10 produces a nearly threefold increase in σ_a. The effect of increasing the K_f of the pore fluid is shown in Fig. 6. Large changes in σ_a are achieved only if $K' < 1$. Increasing K' from 1 to 10 increases σ_a by less than 20 percent. The fact that blood and tissue have nearly the same conductivity, therefore, does not significantly reduce the effectiveness of blood tissue heat transfer. Finally, Fig. 7 shows that the eccentricity of the pore does not significantly affect σ_a and this result is nearly independent of K'.

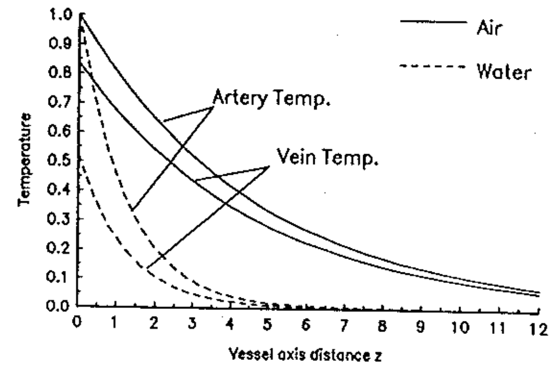

Fig. 8 Temperature distribution along artery-vein axes in both air and water environments. $(\xi_a, \eta_a) = (-2,0)$, $(\xi_v, \eta_v) = (1,0)$, $\rho_{vr} = 1.6$ and $V_v/V_a = -1/1.6^2$

(c) Rat Cremaster Muscle. A representative solution for countercurrent flow in a first generation artery-vein pair in rat cremaster muscle is shown in Fig. 8. For this calculation we have chosen $2D/H = 32$ to insure that the adiabatic boundary condition at $x = \pm D$ is accurately satisfied. A typical vessel tissue geometry for the rate cremaster muscle is: artery diameter, 120 μm, vein diameter, 200 μm, and tissue thickness, 300 μm. The ratio of artery to vein velocity is determined by requiring that the mass flow in each vessel be the same. Both air and water environments are examined. For air, $K_{air} = 0.02622$ W/m°C, $h_{air} = 13.34$ W/m^2°C and $Bi_{air} = 0.00134$. For water, $K_{water} = 0.5967$ W/m°C, $h_{water} = 235.525$ W/m^2°C and $Bi_{water} = 0.0237$. The inlet boundary conditions are $\theta_{ab} = 1$ at $z = 0$ and $\theta_{vb} = 0$ at $z = 20$. This calculation is used to guide the design of our rat cremaster muscle experiments. The feasibility of this experiment rests on our ability to detect measurable temperature disturbances at significant distances from the entrance of the artery in the cremaster tissue preparation and on the ability to measure the local difference in temperature between vessels in the artery-vein pair. This feasibility is demonstrated by the solution shown in Fig. 8, which shows the temperature decay in the vessel direction. The solution predicts that measurable thermal disturbances in a water bath preparation are confined to a dimensionless distance $z = 4$, or a physical distance z^* that is $4Pe\rho_{ar}^*$. Significant artery-vein temperature differences can likewise be detected over this distance. For a 120 μm diameter artery with Pe = 5 this decay length is only 1 mm [15]. Although this distance can be increased or decreased by pharmacologically induced changes in diameter and consequently blood flow in the cremaster muscle that either increase or decrease $Pe\rho_{ar}^*$, this distance is too short to be observed by high resolution infrared thermography. However, the model predicts in Fig. 8 that if the water is drained from the bath and briefly exposed to the air the thermal equilibration length is about four times larger. The latter experimental design has been employed in [15] to obtain the first experimental measurements of axial countercurrent thermal equilibration lengths in a microvascular tissue preparation. Obviously, in smaller vessels downstream there is almost no temperature difference across the tissue layer, since the blood has already reached equilibrium with the surrounding tissue in the larger vessels upstream. These calculations suggest that thermal equilibration occurs primarily in the 1A and 2A vessels of the rat cremaster muscle except at very high non-physiological flow rates. The first measurements of the thermal responses of 1A to 4A vessels to heating and the predicted increase in k_{eff} for the rat cremaster muscle is presented in [16].

6 Concluding Remarks

Although the continuity of heat flux on the vessel surface is satisfied only globally when $K' \neq 1$ by the approximate solution presented herein, this solution, which is exact for $K' = 1$ is highly accurate for $K' \neq 1$ for a wide range of geometry and engineering parameters. Since the eccentricity of the vessels is the main factor affecting the accuracy of this solution, there should be negligible error caused by other parameters when the eccentricity $Sa < 1$. Even for large eccentricity, the maximum error in the shape factor was found to be less than 3 percent.

This solution approach is readily extended to two or more vessels with arbitrary K'. Although the accuracy of the approximate solution has been estimated based on a single vessel in a periodic array, errors of the same order are anticipated for more than one embedded vessel since the solution is a superposition of Green's functions using the same fundamental solution.

Although the present calculations have assumed an axially uniform vessel cross section in solving for the axial temperature distribution, the solution procedure can be extended to embedded vessels where both ρ_{ar}^* and H vary axially provided this variation is gradual. One can, therefore, treat branching and tapered vessels or tapered fins. Even though our present motivation stems largely from a need to have a better understanding of countercurrent microvascular heat transfer, the solutions for the single vessel periodic array provide important new insight into the enhancement in heat transfer that can be achieved by the proper design of fluted fins and microchips with internal convective pores. The solutions, therefore, are of much broader engineering utility.

Finally, the numerical solution in Section 3A is highly efficient since the series solution converges rapidly and the unknown coefficients involve the numerical integration of single integrals that are not singular. Complete solutions can be obtained for a countercurrent pair using a few minutes of CPU time on a small computer. Furthermore, the solution for the heat transfer shape factor involves only a single unknown coefficient given by a single integral which is easily calculated.

Acknowledgment

The first author would like to express here sincere appreciation to Profs. L. M. Jiji and D. Lemons for many helpful comments and Dr. Yu Zeng for her valuable help in developing the numerical solution scheme. This work was supported by NSF grant CBT-8702582 and NIH grant 5R01 HL2609.

References

1 Weinbaum, S., Jiji, L. M., and Lemons, D. E., "Theory and Experiment for the Effect of Vascular Microstructure on Surface Tissue Heat Transfer—Part 1: Anatomical Foundation and Model Conceptualization," ASME Journal of Biomechanical Engineering, Vol. 106, 1984, pp. 321–330.

2 Weinbaum, S., and Jiji, L. M., "A New Simplified Bioheat Equation for the Effect of Blood Flow on Local Average Tissue Temperature," ASME Journal of Biomechanical Engineering, Vol. 107, 1985, pp. 131–139.

3 Lemons, D. E., Chien, S., Crawshaw, L. I., Weinbaum, S., and Jiji, L. M., "The Significance of Vessel Size and Type in Vascular Heat Transfer," *Am. J. Physiol.*, Vol. 253, 1987, pp. R128–135.

4 Chen, M. M., and Holmes, K. R., "Microvascular Contributions in Tissue Heat Transfer," *Ann. N. Y. Acad. Sci.*, Vol. 335, 1980, pp. 137–150.

5 Chato, J., "Heat Transfer to Blood Vessels," ASME Journal of Biomechanical Engineering, Vol. 102, 1980, pp. 110–118.

6 Hahne, E., and Grigull, U., "A Shape Factor Scheme for Point Source Configurations," *Int. J. Heat Mass Transfer*, Vol. 17, 1974, pp. 267–273.

7 Thiyagarajan, R., and Yovanovich, M. M., "Thermal Resistance of a Buried Cylinder with Constant Flux Boundary Condition," ASME *Journal of Heat Transfer*, Vol. 96, 1974, pp. 249–250.

8 Bau, H. H., and Sadhal, S. S., "Heat Losses from a Fluid Flowing in a Buried Pipe," *Int. J. Heat Mass Transfer*, Vol. 25, 1982, pp. 1621–1629.

9 DiFelice, R. F., Jr., and Bau, H. H., "Conductive Heat Transfer Between Eccentric Cylinders with Boundary Conditions of the Third Kind," ASME *Journal of Heat Transfer*, Vol. 105, 1983, pp. 678–680.

10 Baish, J. W., Ayyaswamy, P. S., and Foster, K. R., "Small-scale Temperature Fluctuations in Perfused Tissue During Local Hyperthermia," ASME Journal of Biomechanical Engineering, Vol. 108, 1986, pp. 246–250.

11 Zhu, M., Weinbaum, S., Jiji, L. M., and Lemons, D. E., "On the Generalization of the Weinbaum-Jiji Bioheat Equation to Microvessels of Unequal Size: the Relation Between the Near Field and Local Average Tissue Temperatures," ASME Journal of Biomechanical Engineering, Vol. 110, 1988, pp. 74–81.

12 Zhu, M., Weinbaum, S., and Jiji, L. M., "Heat Exchange Between Unequal Countercurrent Vessels Asymmetrically Embedded in a Cylinder with Surface Convection," *Int. J. Heat Mass Transfer*, Vol. 33, 1990, pp. 2275–2284.

13 Wissler, E. H., "An Analytical Solution Countercurrent Heat Transfer Between Parallel Vessels with a Linear Axial Temperature Gradient," ASME Journal of Biomechanical Engineering, Vol. 110, 1988, pp. 254–256.

14 Wu, Y. L., Weinbaum, S., and Jiji, L. M., "A New Analytic Technique for 3-D Heat Transfer from a Cylinder with Two or More Axially Interacting Eccentrically Embedded Vessels with Application to Countercurrent Blood Flow," *Int. J. Heat Mass Transfer*, Vol. 36, 1993, pp. 1073–1083.

15 Zhu, L., Lemons, D. E., and Weinbaum, S., "Microvascular Thermal Equilibration in Rat Cremaster Muscle," submitted to *Phys. Med. Biol.* (1995).

16 Zhu, L., Lemons, D. E., and Weinbaum, S., "A New Approach for Predicting the Enhancement in the Effective Conductivity of Perfused Muscle Tissue Due to Hyperthermia," *Annals of Biomedical Engineering*, in press (1995).

APPENDIX 1

In this Appendix we shall derive the Green's function $W(x,y:\xi,\eta)$ for a line source at $x = \xi$, $y = \eta$ that is described by Eqs. (14) and (33) in the text. The governing equation and boundary conditions for W are the following:

$$\nabla^2 W(x,y:\xi,\eta) = \delta(x-\xi)\delta(y-\eta)$$

$$y = H_1, \qquad \frac{\partial W}{\partial y} = -\mathrm{Bi}_1 W$$

$$y = -H_2, \qquad \frac{\partial W}{\partial y} = -\mathrm{Bi}_2 W$$

$$x = \pm D, \qquad \frac{\partial W}{\partial x} = 0$$

We assume that $W(x,y:\xi,\eta)$ can be written in the separable form,

$$W(x,y:\xi,\eta) = \sum_{n=0}^{\infty} X_n(x) Y_n(y:\xi,\eta) \qquad (A.1)$$

where $X_n(x)$ satisfies

$$\frac{d^2X_n(x)}{dx^2} = -\lambda_n X_n(x)$$

$$x = \pm D, \quad \frac{dX_n(x)}{dx} = 0 \qquad (A.2)$$

The eigenfunction $X_n(x)$ is obtained as

$$X_0(x) = 1, \qquad \lambda_0 = 0 \qquad n = 0$$

$$X_n(x) = \cos\left[\sqrt{\lambda_n}\,(x - D)\right], \quad \lambda_n = \left(\frac{n\pi}{2D}\right)^2, \qquad n = 1,2,\ldots\infty \quad (A.3)$$

Substituting $(A.3)$ into $(A.1)$, we obtain

$$\sum_{n=0}^{\infty}\left[\frac{d^2Y_n(y:\xi,\eta)}{dy^2} - \lambda_n Y_n(y:\xi,\eta)\right]\cos\left[\sqrt{\lambda_n}\,(x - D)\right] = \delta(x-\xi)\delta(y-\eta) \quad (A.4)$$

Multiplying both sides of Eq. $(A.4)$ by $\cos[\sqrt{\lambda_n}(x - D)]$ and integrating from $-D \le x \le D$, we obtain

$$\frac{d^2Y_0}{dy^2} = \frac{1}{2D}\delta(y-\eta) \qquad n = 0 \qquad (A.5)$$

$$\frac{d^2Y_n}{dy^2} - \lambda_n Y_n = \frac{\cos\left[\sqrt{\lambda_n}\,(\xi - D)\right]}{D}\delta(y-\eta) \qquad n = 1,2,3\ldots \quad (A.6)$$

Equation $(A.5)$ and its boundary condition can also be written as

$$\frac{d^2Y_0}{dy^2} = 0 \qquad \text{at } y \neq \eta$$

$$\frac{dY_0}{dy}\Big|_{y=\eta^+} - \frac{dY_0}{dy}\Big|_{y=\eta^-} = \frac{1}{2D}, \quad Y_0|_{y=\eta^+} = Y_0|_{y=\eta^-}$$

$$\frac{dY_0}{dy} = -\mathrm{Bi}_1 Y_0 \qquad \text{at } y = H_1$$

$$\frac{dY_0}{dy} = \mathrm{Bi}_2 Y_0 \qquad \text{at } y = -H_2 \qquad (A.7)$$

The solution of the boundary value problem $(A.7)$ for Y_0 is

$$Y_0(y:\xi,\eta) = C_1 y + C_2 \qquad \eta \le y \le H_1$$

$$Y_0(y:\xi,\eta) = D_1 y + D_2 \qquad -H_2 \le y \le \eta \quad (A.8)$$

where

$$C_1 = \left(\eta - H_2 + \frac{1}{\mathrm{Bi}_2}\right)\Big/\left[2D\left(H_1 + H_2 + \frac{1}{\mathrm{Bi}_1} + \frac{1}{\mathrm{Bi}_2}\right)\right]$$

$$D_1 = \left(\eta - H_1 - \frac{1}{\mathrm{Bi}_1}\right)\Big/\left[2D\left(H_1 + H_2 + \frac{1}{\mathrm{Bi}_1} + \frac{1}{\mathrm{Bi}_2}\right)\right]$$

$$C_2 = -C_1\left(H_1 + \frac{1}{\mathrm{Bi}_1}\right)$$

$$D_2 = D_1\left(H_2 + \frac{1}{\mathrm{Bi}_2}\right)$$

Similarly, the boundary value problem for Y_n in Eq. $(A.6)$ can be written as

$$\frac{d^2Y_n}{dy^2} - \lambda_n Y_n = 0 \qquad \text{at } y \neq \eta$$

$$\frac{dY_n}{dy}\Big|_{y=\eta^+} - \frac{dY_n}{dy}\Big|_{y=\eta^-} = \frac{\cos\left[\sqrt{\lambda_n}\,(\xi - D)\right]}{D},$$

$$Y_n|_{y=\eta^+} = Y_n|_{y=\eta^-}$$

$$\frac{dY_n}{dy} = -\mathrm{Bi}_1 Y_n \qquad \text{at } y = H_1$$

$$\frac{dY_n}{dy} = \mathrm{Bi}_2 Y_n \qquad \text{at } y = -H_2 \qquad (A.9)$$

The solution for Y_n is:

$$Y_n(y:\xi,\eta) = \frac{\cos\left[\sqrt{\lambda_n}\,(\xi - D)\right]}{D}\left[A_1 e^{\sqrt{\lambda_n}y} + B_1 e^{-\sqrt{\lambda_n}y}\right] \qquad y \ge \eta$$

$$Y_n(y:\xi,\eta) = \frac{\cos\left[\sqrt{\lambda_n}\,(\xi - D)\right]}{D}\left[A_2 e^{\sqrt{\lambda_n}y} + B_2 e^{-\sqrt{\lambda_n}y}\right] \qquad y < \eta \quad (A.10)$$

where

$$P_1 = \left(\sqrt{\lambda_n} + \mathrm{Bi}_1\right)/\left(\sqrt{\lambda_n} - \mathrm{Bi}_1\right)$$

$$P_2 = \left(\sqrt{\lambda_n} - \mathrm{Bi}_2\right)/\left(\sqrt{\lambda_n} + \mathrm{Bi}_2\right)$$

$$A_1 = \frac{1}{2\sqrt{\lambda_n}}\frac{1 + P_2 e^{-\sqrt{\lambda_n}(2H_2+2\eta)}}{\left[-P_1 + P_2 e^{-\sqrt{\lambda_n}(2H_2+2H_1)}\right]}e^{-\sqrt{\lambda_n}(2H_1-\eta)}$$

$$B_1 = \frac{1}{2\sqrt{\lambda_n}}\frac{1 + P_2 e^{-\sqrt{\lambda_n}(2H_2+2\eta)}}{\left[-P_1 + P_2 e^{-\sqrt{\lambda_n}(2H_2+2H_1)}\right]}P_1 e^{\sqrt{\lambda_n}\eta}$$

$$A_2 = \frac{1}{2\sqrt{\lambda_n}}\frac{P_1 + e^{-\sqrt{\lambda_n}(2H_1-2\eta)}}{\left[-P_1 + P_2 e^{-\sqrt{\lambda_n}(2H_2+2H_1)}\right]}e^{\sqrt{\lambda_n}\eta}$$

$$B_2 = \frac{1}{2\sqrt{\lambda_n}}\frac{P_1 + e^{-\sqrt{\lambda_n}(2H_1-2\eta)}}{\left[-P_1 + P_2 e^{-\sqrt{\lambda_n}(2H_2+2H_1)}\right]}P_2 e^{-\sqrt{\lambda_n}(2H_2+\eta)}$$

Substituting $(A.8)$ and $(A.10)$ into $(A.1)$, we obtain the following expressions for the Green's function $W(x,y:\xi,\eta)$, which are used in Sections 3 and 4,

$$W = (C_1 y + C_2) + \sum_{n=1}^{\infty}\frac{1}{D}\cos\left[\sqrt{\lambda_n}\,(\xi - D)\right] \times\cos\left[\sqrt{\lambda_n}\,(x - D)\right]\left[A_1 e^{\sqrt{\lambda_n}y} + B_1 e^{-\sqrt{\lambda_n}y}\right] \qquad y \ge \eta$$

$$W = (D_1 y + D_2) + \sum_{n=1}^{\infty}\frac{1}{D}\cos\left[\sqrt{\lambda_n}\,(\xi - D)\right] \times\cos\left[\sqrt{\lambda_n}\,(x - D)\right]\left[A_2 e^{\sqrt{\lambda_n}y} + B_2 e^{-\sqrt{\lambda_n}y}\right] \qquad y < \eta \qquad (A.11)$$

where $(A.11)$ are Eqs. $(33a,b)$ in the text.

If the source is located at $\xi = \eta = 0$, the expressions for the Green's function simplifies to:

$$W = (C_1 y + C_2) + \sum_{n=1}^{\infty} \frac{1}{D} \cos\left[\frac{n\pi}{2}\right] \times \cos\left[\sqrt{\lambda_n}(x - D)\right]\left[A_1 e^{\sqrt{\lambda_n} y} + B_1 e^{-\sqrt{\lambda_n} y}\right] \quad y \geq \eta$$

$$W = (D_1 y + D_2) + \sum_{n=1}^{\infty} \frac{1}{D} \cos\left[\frac{n\pi}{2}\right] \times \cos\left[\sqrt{\lambda_n}(x - D)\right]\left[A_2 e^{\sqrt{\lambda_n} y} + B_2 e^{-\sqrt{\lambda_n} y}\right] \quad y < \eta \qquad (A.12)$$

(A.12) are Eqs. (14a,b) in the text.

APPENDIX 2

In this Appendix we shall show that Eq. (19) is valid only when the ratio $K' = 1$. This proof rests on the use of Green's theorem.

If we decompose K' into two terms, 1 and $K' - 1$, the left side of (19) becomes

$$\frac{C_{sa}}{\pi}\int_{-\pi}^{\pi}\left[\frac{W(\rho_a,\phi_a{:}0,0)}{\rho_a^j} - \frac{\partial W(\rho_a,\phi_a{:}0,0)}{\partial\rho_a}\frac{1}{j\rho_a^{j-1}}\right] \times \cos(j\phi_a)|_{\rho_a=1} d\phi_a + \frac{(K'-1)C_{sa}}{\pi} \times \int_{-\pi}^{\pi} W(\rho_a,\phi_a{:}0,0)\frac{\cos(j\phi_a)}{\rho_a^j}|_{\rho_a=1} d\phi_a \qquad (A.13)$$

The first integral in Eq. (A.13) can also be written as

$$\frac{C_{sa}}{\pi}\oint_{\Gamma}\left[\rho_a^{j-1}\cos(j\phi_a)W(\rho_a,\phi_a{:}0,0) - \frac{\rho_a^j}{j}\cos(j\phi_a)\frac{\partial W(\rho_a,\phi_a{:}0,0)}{\partial\rho_a}\right]|_{\rho_a=1} d\Gamma, \qquad (A.14)$$

where Γ is the vessel surface $\rho_a = 1$. Considering that $\partial[\rho_a^j\cos(j\phi_a)/j]/\partial\rho_a = \rho_a^{j-1}\cos(j\phi_a)$ and applying Green's theorem to expression (A.14), one obtains

$$\iint_{\Omega}\left\{W(\rho_a,\phi_a{:}0,0)\nabla^2\left[\frac{\rho_a^j}{j}\cos(j\phi_a)\right] - \frac{\rho_a^j}{j}\cos(j\phi_a)\nabla^2 W(\rho_a,\phi_a{:}0,0)\right\}d\Omega = \iint_{\Omega}\left\{-\frac{\rho_a^j}{j}\cos(j\phi_a)\nabla^2 W(\rho_a,\phi_a{:}0,0)\right\}d\Omega \qquad (A.15)$$

where Ω refers to the region inside the vessel. Since the Green's function $W(\rho_a,\phi_a{:}0,0)$ satisfies Laplace's equation within Γ except at the source point, expression (A.15) reduces to

$$\left[\frac{\rho_a^j}{j}\cos(j\phi_a)\right]|_{\rho_a=0} = 0$$

The above derivation shows that the first integral in (A.13) vanishes for any j. The second integral in (A.13) is the integral of the Green's function multiplied by the weighting function $\cos(j\phi_a)$. This integral is equal to zero for any j only if the Green's function is a constant, which is not the case. Only when $K' = 1$ does this second term vanish for any j. Since the left side of (19) and (A.13) are equivalent, Eq. (19) is valid for all j only when $K' = 1$.